

Article

Flexible Modulation of Perfect Vortex Beams by Combining Coherent Beams

Bowang Shu ¹, Yuqiu Zhang ^{1,*}, Hongxiang Chang ¹, Shiqing Tang ¹, Jinyong Leng ^{1,2,3}, Jiangming Xu ¹ and Pu Zhou ^{1,*}

¹ College of Advanced Interdisciplinary Studies, National University of Defense Technology, Changsha 410000, China; shubowang17@nudt.edu.cn (B.S.); changhongxiang18@nudt.edu.cn (H.C.); tsq18@nudt.edu.cn (S.T.); lengjinyong07@nudt.edu.cn (J.L.); jmxu1988@nudt.edu.cn (J.X.)

² Nanhu Laser Laboratory, National University of Defense Technology, Changsha 410000, China

³ Hunan Provincial Key Laboratory of High Energy Laser Technology, National University of Defense Technology, Changsha 410000, China

* Correspondence: zhangyq914@163.com (Y.Z.); zhoup203@163.com (P.Z.)

Abstract: Perfect vortex beams (PVBs) possess the advantage of a stable light field distribution regardless of their topological charges, and thus they are extensively utilized in various applications, such as free-space optical communication, optical tweezers and laser processing. Herein, we report a new strategy to generate and modulate PVBs using coherent beam combining (CBC) technology. Both piston phase and tilting phase controlling methods have been successfully employed, and the corresponding properties of the generated PVBs have been fully investigated. Moreover, the number and position of the gaps in fractional perfect vortex beams (FPVBs) could be precisely controlled, and the relationships between these modulated parameters and the performance of FPVBs are uncovered. These simulation analysis results demonstrate the potential for flexible modulation of PVBs or FPVBs in the CBC system, indicating promising prospects for coherent beam arrays (CBAs) in laser beam shaping and achieving high-power structured light.

Keywords: perfect vortex vortices; coherent beam combining; fractional perfect vortex beams; orbital angular momentum mode purity



Citation: Shu, B.; Zhang, Y.; Chang, H.; Tang, S.; Leng, J.; Xu, J.; Zhou, P. Flexible Modulation of Perfect Vortex Beams by Combining Coherent Beams. *Photonics* **2024**, *11*, 385. <https://doi.org/10.3390/photonics11040385>

Received: 21 March 2024

Revised: 12 April 2024

Accepted: 17 April 2024

Published: 18 April 2024



Copyright: © 2024 by the authors. Licensee MDPI, Basel, Switzerland. This article is an open access article distributed under the terms and conditions of the Creative Commons Attribution (CC BY) license (<https://creativecommons.org/licenses/by/4.0/>).

1. Introduction

In 2013, Ostrovsky et al. first reported the concept of a perfect vortex beam (PVB) [1,2], and it has aroused much attention due to its consistent diameter despite variations in the topological charge [3]. Such a property of PVBs should be highlighted, as it has many advantages in expanding the applications of optical communication [4–6]. Moreover, fractional perfect vortex beams (FPVBs) even provide significant possibilities in high-dimensional encoding technology for optical communication [7] and facilitate particle manipulations as optical tweezers [8]. Inspired by these potential applications, various pathways of developing optical vortices and their remarkable properties have been investigated in depth [9,10]. There are also several efficient methods to generate PVBs, such as optimal phase elements, transformation via Bessel–Gaussian (BG) beams and so on [11,12]. Among them, the crucial procedure is the interconversion between PVBs and BG beams, indicating that PVBs could be formed based on BG beams, which are easily obtained using axicon lenses or the Bessel beam kinoform [13]. Recently, PVBs have been modulated with designed phase patterns, resulting in abundant shapes and special characteristics, and these transformations have been proven to be robust in diverse applications [14,15].

However, most of the methods are based on a typical device called a spatial light modulator, which is unable to support the requirements of power scaling. The challenges from the aspect of a limited output power hinder the development of this structured light to some extent. As we know, coherent beam combining (CBC) technology has been

rapidly developed for light field modulation due to its abundant modulable dimensions, for example, amplitude, phase, polarization, etc. [16–18]. Note that most indexes of structured light generated by coherent beam arrays (CBAs) have been greatly improved recently. As reported by Long et al., 1.5 kW high-power fractional vortex beams (FVB) have been experimentally realized using a CBC system [19]. Additionally, orbital angular momentum (OAM) beam generation has been reported by Veinhard, M. et al. with a 61-channel femtosecond digital laser [20]. Owing to efficient controlling strategies, CBC technology is a potential solution to solve the problem of the harsh requirements on power scaling.

Up to now, various kinds of structured beams generated by utilizing CBC systems have been reported, including vectorial beams [21,22], Airy beams [23], BG beams [24,25] and so on. As reported by Chu et al., in 2015, BG beams were achieved using a single circular arrangement of a CBA [26]. Later, in 2020, Yu et al. verified such a phenomenon both theoretically and experimentally [25]. Based on these findings, it is possible to obtain PVBs by introducing optimal elements for Fourier transformations in a CBC system. Then, in 2023, Ju et al. reported the successful creation of perfect vectorial vortex beams and investigated the corresponding phase control scheme based on CBC technology theoretically [27,28]. The architecture of a CBA is composed of adjacent apertures with different polarization states. However, related works are mainly concentrated on the generation of PVBs, and examples of modulated PVBs or FPVBs with variable forms generated via the CBC technique are still limited. This point remains a challenging task in practical application [29,30]. Thus, it is crucial to thoroughly investigate the corresponding methods in order to enrich the forms of structured light, which is expected to expand the possibilities of laser beam shaping by a CBC system.

In this study, PVBs have been successfully generated by employing CBC technology. We utilize two methods to control the near-field phase in a CBA: one involves employing a conventional piston phase to simulate the spiral phase, while the other entails implementing a tilting phase that is similar to the axicon phase. Based on these two methods, PVBs with a high OAM mode purity have been obtained via spatial filtering. Moreover, the relationships underlying the modulated parameters and properties of PVBs have been uncovered. Not only it is shown that FPVBs are freely transformed by FVBs, but also that the location and numbers of the gaps of the FPVBs are precisely controlled. Hence, this work reveals that a CBC system is a reasonable choice to solve the problems of inflexible beam shaping of PVBs or FPVBs, which is expected to be further used in advanced applications.

2. Simulation Analysis Methods

This section illustrates the simulation analysis method of generation and modulation of PVBs. Considering a CBA is constructed by N apertures in a circular arrangement (as seen in Figure 1), the complex amplitude distribution in the (x_1, y_1) incident plane can be described as:

$$E(x_1, y_1) = \sum_n^N A_n = \sum_n^N \exp\left[-\frac{(x_1 - a_n)^2 + (y_1 - b_n)^2}{w_0^2}\right] \times \exp(il\theta_n + \Delta\varphi) \times \text{circ}\left[\frac{\sqrt{(x_1 - a_n)^2 + (y_1 - b_n)^2}}{d_0/2}\right] \tag{1}$$

where w_0 is the radius of each Gaussian-shaped beamlet and d_0 is the diameter of each aperture. Then, (a_n, b_n) is the central coordinate of the n -th beamlet, where $a_n = R \cos \theta_n$ and $b_n = R \sin \theta_n$. Herein, θ_n represents the piston phase in each aperture, and it can be written as $\theta_n = \frac{2\pi n}{N}$. Meanwhile, l is assigned as the topological charge, and it can be an integer or fraction, decided by the type of the structured beams. If FVBs are required, the topological charge will be set to $l + 0.5$. To decide the positions of the gaps in the FPVBs, $\Delta\varphi$ represents the phase difference. For convenience, $T = \text{circ}\left[\frac{\sqrt{(x_1 - a_n)^2 + (y_1 - b_n)^2}}{d_0/2}\right]$ will be used in the following formula.

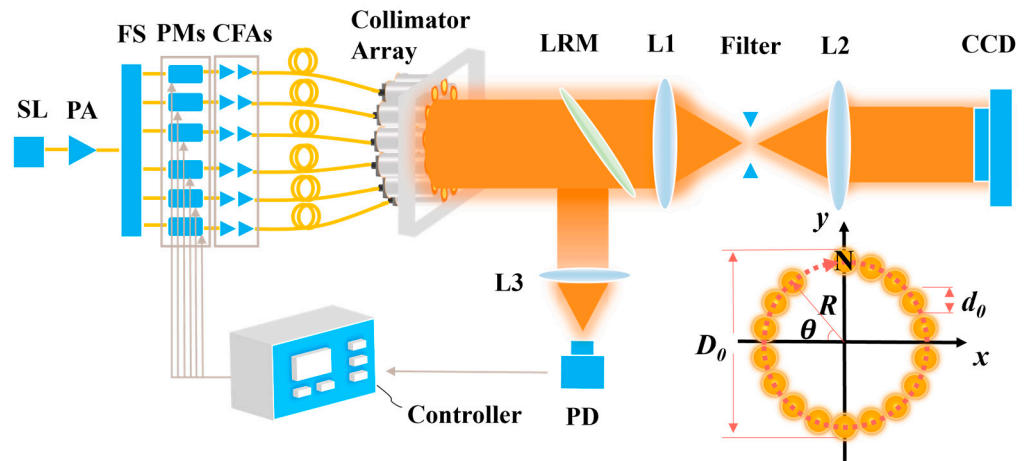


Figure 1. Schematics of a CBC system for generation and modulation of PVBs or FPVBs. Inset: near-field amplitude distribution.

To prove that BG beams could be generated by a CBA, Formula (1) should be further studied. For ease of derivation, the cartesian coordinate system (x_1, y_1) is transferred to a polar coordinate system (r_1, φ_1) , and Formula (1) can be expressed as:

$$E(x_1, y_1) = \sum_n^N T \exp\left[-\frac{r_1^2 + R^2}{w_0^2}\right] \times \exp\left[-\frac{2Rr_1 \cos(\varphi_1 - \theta_n)}{w_0^2}\right] \times \exp(il\theta_n) \quad (2)$$

where R represents the radius of the whole circularly arranged CBA. By utilizing the approximation of $\Delta\theta = \Delta\left(\frac{2\pi n}{N}\right) = \frac{2\pi}{N}\Delta n$, then $d\theta = \frac{2\pi}{N}dn$. If N is large enough, Formula (2) can be further written as:

$$E(x_1, y_1) \approx \frac{N}{2\pi} \exp\left[-\frac{r_1^2 + R^2}{w_0^2}\right] \int_0^{2\pi} T \exp\left[-\frac{2Rr_1 \cos(\varphi_1 - \theta)}{w_0^2}\right] \times \exp(i\theta) d\theta \quad (3)$$

As we know, the standard integral and Bessel function identity is represented by $J_l(p) = \frac{1}{2\pi} \int_0^{2\pi} \exp(p \cos \varphi - il\varphi) d\varphi$ [23], and Formula (3) can finally be expressed as:

$$E(x_1, y_1) = N \exp\left[-\frac{r_1^2 + R^2}{w_0^2}\right] J_l\left(\frac{2Rr_1}{w_0^2}\right) \exp(il\varphi_1) \quad (4)$$

which is equivalent to the form of a BG light field distribution.

During free-space propagation, spatial filtering is an established method to improve the beam quality by removing the unwanted high-frequency noise. Due to the characteristics of a structured light field generated via a CBC system, Bessel–Gaussian beams with a typical ring structure could be realized by spatial filtering. In the focal plane (x_2, y_2) , we express the complex amplitude distribution as follows:

$$E(x_2, y_2) \approx \frac{\exp(i4\pi f/\lambda)}{if\lambda} F\{E(x_1, y_1)\} \text{circ}\left(\sqrt{x_2^2 + y_2^2}/d_f\right) \quad (5)$$

where d_f represents the filtering threshold in this work. Lastly, PVBs can be achieved via Fourier transform of $E(x_2, y_2)$. With the designed filtering threshold, the OAM mode purity of the generated PVBs will be improved. Note that the determination of the filtering threshold is related to the ring width of the Bessel–Gaussian beams, and PVBs could be generated if the complete ring is cut off.

If the controlling method is chosen to be the tilting phase, the complex amplitude distribution in the (x_1, y_1) incident plane can be described as:

$$E_t(x_1, y_1) = \sum_n^N A_n = \sum_n^N \exp\left[-\frac{(x_1 - a_n)^2 + (y_1 - b_n)^2}{w_0^2}\right] \times \exp(i\phi) \times \text{circ}\left[\frac{\sqrt{(x_1 - a_n)^2 + (y_1 - b_n)^2}}{d_0/2}\right] \quad (6)$$

where $\phi = 2\pi r_1/r + l\phi_1$, and r means the periods of phase change. If FPVBs are required by employing a tilting phase, the corresponding phase will be set to ϕ multiplied by a fraction.

3. Results and Discussion

Based on the above simulation analysis method, the schematic of a CBC system for the generation of PVBs is displayed in Figure 1. The light source for the high-power laser output is similar to a typical CBC system, and consists of a seed laser (SL), a pre-amplifier (PA), a fiber splitter (FS), a phase modulator (PM), cascaded fiber amplifiers (CFAs) and a collimator array in turn. Herein, the collimator arrays can be utilized to control the piston phase and the tilting phase, and these two mechanisms are proposed to generate and modulate the PVBs and FPVBs. Then, a low-reflective mirror (LRM) is set to separate a part of laser from the high-power output for phase calibration and compensation, and the controller loaded with the stochastic parallel gradient descent (SPGD) algorithm will be the last procedure of the closed loop. Next, the rest of the laser will pass through lens 1 (L1) and L2, which can be recognized by the spatial filter. Finally, the PVBs or FPVBs will be formed at the focal plane and observed by the charge-coupled device camera (CCD). In this work, we only analyze and discuss the results under ideal conditions. It is assumed that the principles of the generated structured light field are well understood.

3.1. Generation of PVBs by Employing a Piston Phase in a CBC System

With such a designed CBC system, we utilize twenty-four apertures ($N = 24$) in a Gaussian-arranged amplitude and piston phase distribution. With different incident phase distributions, as shown in the insets of Figure 2(a1–a3), different PVBs are formed with topological charges of 1, 2 and 3, and the corresponding far-field intensity and phase are displayed in Figure 2(a1–a3) and Figure 2(b1–b3), respectively. It is obvious that the size of the PVBs produced by different topological charges seems to be unchanged, which is in accordance with the characteristics of PVBs. These results illustrate that a CBA in a single circular arrangement with the designed piston phase could be successfully applied to generate PVBs.

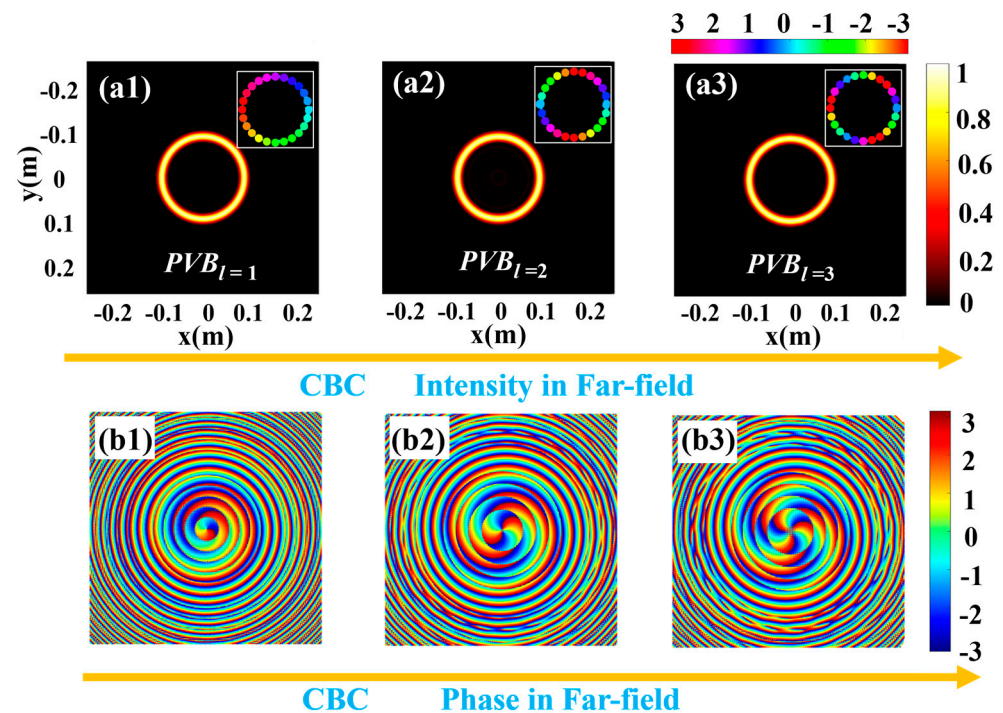


Figure 2. The results of generated PVBs by employing a piston phase in a CBC system. (a1–a3) Far-field intensity distribution. Insets: near-field phase distribution in the CBA. (b1–b3) Far-field phase distribution of generated PVBs with varied topological charges of 1, 2 and 3.

Theoretically, the PVBs are obtained by Fourier transform of BG beams. In detail, the BG beams will be formed before the lens first. Due to the arrayed architecture of the emitting source, the corresponding intensity distribution of BG beams ($l = 1, 2$ and 3) is usually accompanied by sidelobes, as shown in Figure 3(a1,b1,c1), respectively. At the same time, the phenomenon of residual sidelobes has a serious effect on the generation of PVBs, which means spatial filtering should be adopted in consideration of this circumstance. After truncation of the diaphragm, the radially arranged concentric annulus is equivalent to a practical BG light field. As displayed in Figure 3(a2–a4), the interceptive BG beams ($l = 1$) are shown at different filtering thresholds of 0.074, 0.062 and 0.051 m, respectively. Due to the varied BG light field, the parameters of the PVBs will be influenced, especially the diameter, which can be observed in Figure 3(a5–a7). Meanwhile, BG beams with different topological charges show different sidelobe intensity distributions, which means the filtering threshold should be varied. Under the same condition, the filtering thresholds are chosen as 0.068, 0.056 and 0.044 m when $l = 2$ in Figure 3(b2–b4), and 0.061, 0.048 and 0.037 m when $l = 3$ in Figure 3(c2–c4).

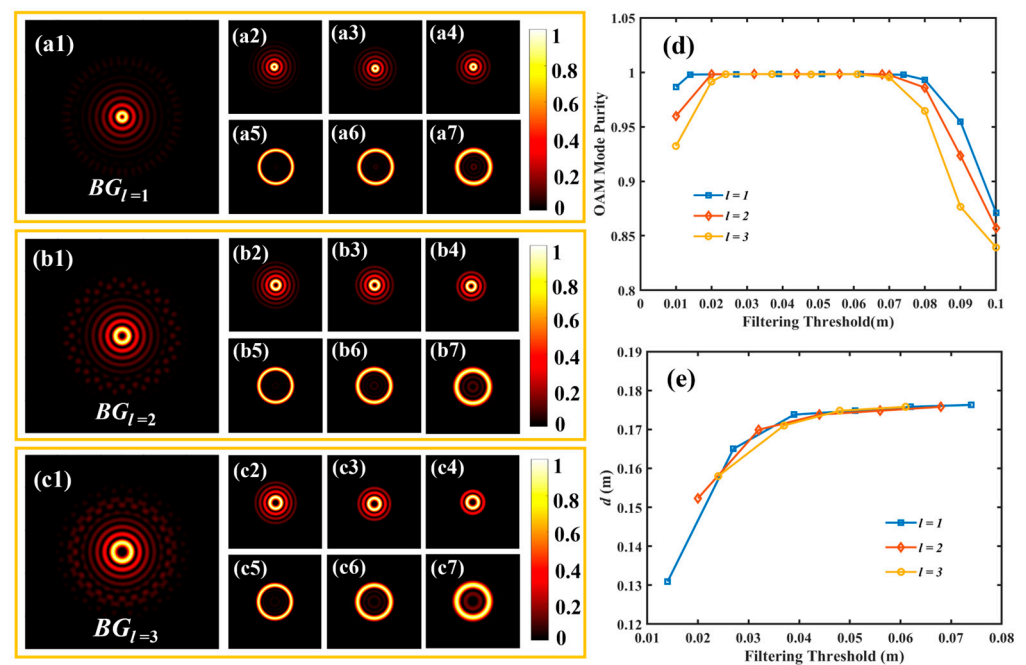


Figure 3. The mechanisms underlying generated PVBs by employing a piston phase in a CBC system. (a1) The generated BG beam as $l = 1$; (a2–a4) interceptive BG beams at filtering thresholds of 0.074, 0.062 and 0.051 m, respectively; (a5–a7) corresponding far-field intensity of PVBs as $l = 1$. (b1) The generated BG beam as $l = 2$; (b2–b4) interceptive BG beams at filtering thresholds of 0.068, 0.056 and 0.044 m, respectively; (b5–b7) corresponding far-field intensity of PVBs as $l = 2$. (c1) The generated BG beam as $l = 3$; (c2–c4) interceptive BG beams at filtering thresholds of 0.061, 0.048 and 0.037 m, respectively; (c5–c7) corresponding far-field intensity of PVBs as $l = 3$. (d) The relationships between the OAM mode purity and filtering thresholds. (e) The relationships between the diameter of PVBs and the filtering thresholds.

These results illustrate that the filtering threshold should be fully considered to realize the desired PVBs. To find out the underlying relationships between the characteristics of PVBs and the filtering threshold, the performances of the generated PVBs can be measured by the OAM mode purity and diameter (d), as depicted in Figure 3d,e, respectively. Note that when the filtering threshold is at a relatively high value, it means that there are more residual sidelobes than that at a lower value. According to the curves in Figure 3d, the OAM mode purity gradually increases as petal-shaped sidelobes are filtered in the outermost layer. In addition, the OAM mode purity displays several peak points (ca. 99.8%) at the stage of BG light field formation. If the structure of the concentric annulus is broken, the

OAM mode purity decreases dramatically. As the number of concentric rings of the BG beams varies from $l = 1$ to 3, the number of peak points reduces. The reason for the achieved high OAM mode purity of PVBs is due to the reasonable filtering thresholds. Owing to the function of mode purity optimization provided by spatial filtering, the required OAM modes could be extracted and high-order mode information could be avoided. Thus, this procedure could efficiently improve the OAM mode purity of PVBs up to near unity. In addition to the OAM mode purity, d is another important parameter that cannot be ignored. At the initial stage, the index d of PVBs exhibits a slow trend towards decreasing due to the slow reduction in the efficient BG light field. Later, when the filtering thresholds become lower, the index d of PVBs undergoes significant changes because of the vanishing BG light field. It is worth noting that the gap between the highest and lowest point is limited to the range of 0.05 m, and it will be narrowed as the topological charges differ from $l = 1$ to 3. This finding reveals that reasonable filtering threshold settings are helpful to generate stable PVBs.

In this work, the size of these PVBs could be adjusted flexibly by tuning the parameters of the CBA in the incident source. When the number of apertures in the incident plane was reduced from 24 to 12, seen in Figure 4(a1–a3), the corresponding radius of PVBs changed from 0.174 m to 0.086 m, seen in Figure 4(b1–b3). As the radius of the Gaussian-shaped beamlets in the incident plane was reduced from 0.008 m to 0.005 m, seen in Figure 4(c1–c3), the corresponding radius of the PVBs changed from 0.07 m to 0.016 m, seen in Figure 4(d1–d3). This finding is helpful to achieve PVBs with a controlled size, which will meet the requirements of diverse applications.

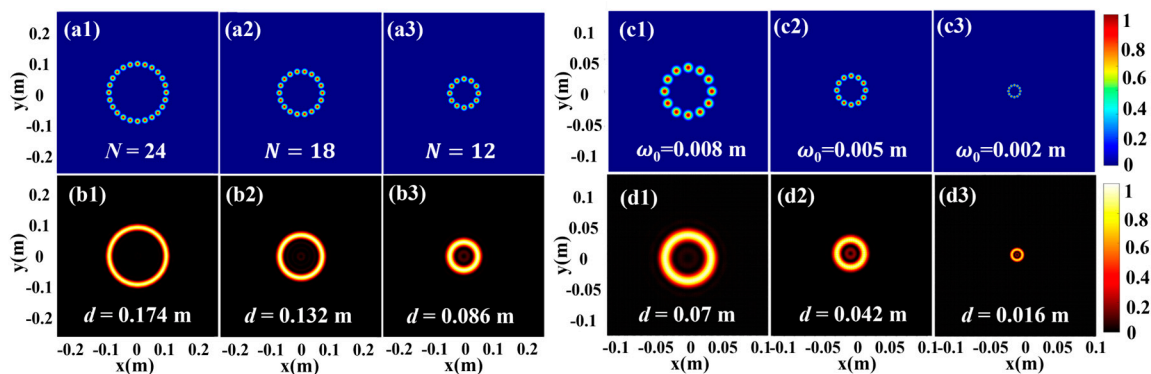


Figure 4. PVBs with a controlled size by tuning the parameters of the aperture. (a1–a3) Near-field intensity distribution of a CBA with different numbers of apertures. (b1–b3) Corresponding far-field intensity distribution of the PVBs. (c1–c3) Near-field intensity distribution of a CBA with different radii of Gaussian-shaped beamlets. (d1–d3) Corresponding far-field intensity distribution of the PVBs.

3.2. Generation and Modulation of FPVBs via a Piston Phase

Previously published work has proven that FVBs can be generated via CBC technology [19]. Furthermore, FPVBs with gaps can be obtained on the basis of modulated FVBs. Herein, the topological charge is set to 1.5 for generation of FPVBs with a single gap using a CBA, and the near-field phase distributions with phase differences of $0, \pi/4, \pi/2, 3\pi/4$ and π are displayed in Figure 5(a1–a5), respectively. The existence of phase differences will decide the positions of gap, and the corresponding far-field intensity diagrams are shown in Figure 5(b1–b5), respectively. To achieve more gaps, the CBA needs to be divided into several groups. For example, the twenty-four apertures are divided into two equal parts, that is, each group is composed of twelve apertures, and the topological charge of each group is also set to 1.5. To control the positions of these two gaps, the phase difference ($\Delta\varphi$) of each group was set to $0, \pi/2, \pi, 3\pi/2$ and 2π , as seen in Figure 5(c1–c5), respectively. Such a configuration of parameters contributes to flexible modulation of FPVBs with more gaps, and the corresponding far-field intensity diagrams are shown in Figure 5(d1–d5),

respectively. Note that the discontinuity in the phase leads to the appearance of countable gaps, which indicates that the prominent split beams in the CBA architecture have advantages for light-field modulation.

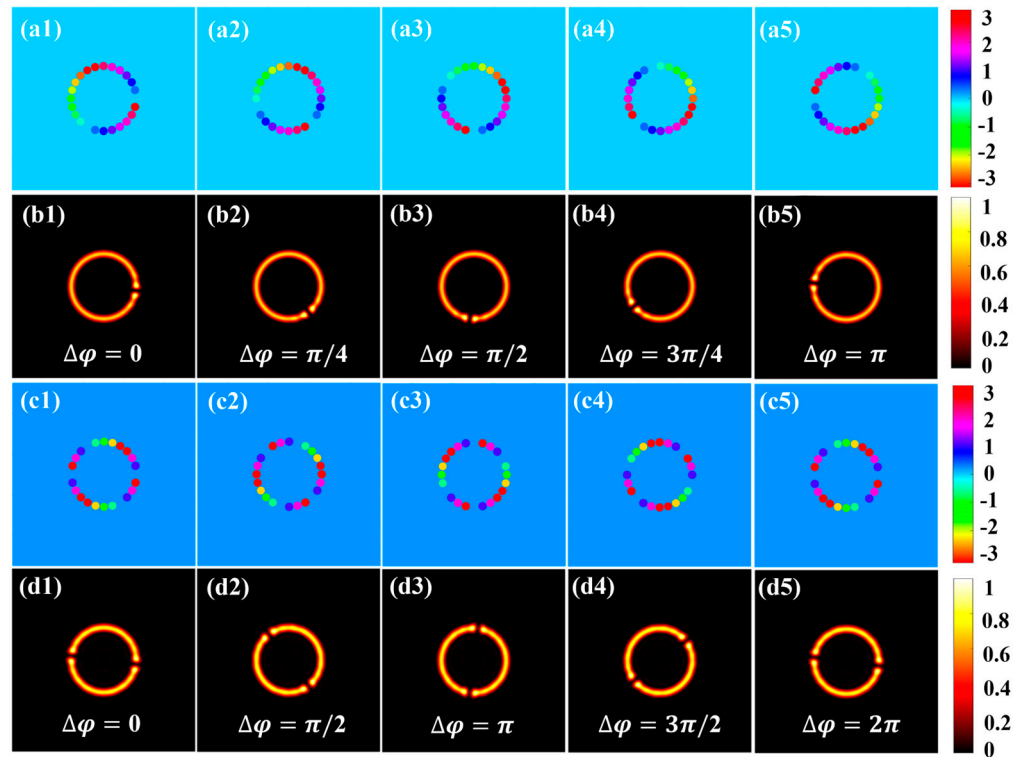


Figure 5. Modulation of FPVBs by employing a piston phase in a CBC system. (a1–a5) Near-field phase distribution; (b1–b5) far-field intensity distribution of an FPVB with a single gap. (c1–c5) Near-field phase distribution; (d1–d5) far-field intensity distribution of an FPVB with two gaps.

To make the rules of FPVB modulation clear, its underlying mechanism should be uncovered. As shown in Figure 6(a1–a4), there is a relationship between the fractional part of the topological charge and the morphology of the gap. It was found that the size of the gap was largest when the fractional part is 0.5, and the size became larger as the numerical value is closer to 0.5. Meanwhile, the number of apertures is important in determining the number of gaps. As shown in Figure 6(b1–b4), these far-field intensity diagrams show that the global intensity distribution seems to be much more uniform if the number of apertures is large enough, especially in the comparison between light field distributions when $N = 24$ and $N = 60$.

To obtain more precise rules, Figure 6(d1,d2) show the results of the far-field intensity distribution with four gaps, and these gaps are formed by 36 apertures in the near field. We divide these apertures into four unequal groups, with one split configuration of 7, 11, 7 and 11, and another of 8, 10, 8 and 10. In comparison with the result in Figure 6(b2), it can be proven that at least nine apertures in one group are satisfactory to generate one single gap. Thus, the maximum number of available gaps can be calculated by $[N/9]$, and more apertures would be better to achieve FPVBs with better performances. The chart in Figure 6c uncovers the relationship between the number of apertures and the maximum number of available gaps. As seen in Figure 6(e1,e2), it can be found that six or eight gaps are successfully modulated by 96 apertures, respectively. Note that these results are provided under the condition of the same filtering threshold of 0.065 m.

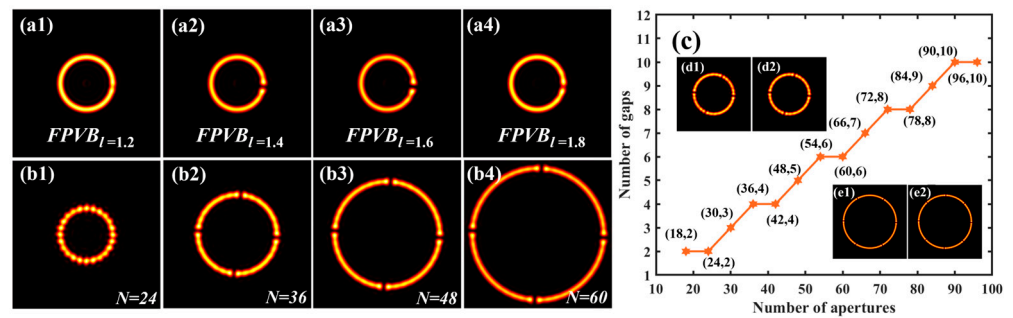


Figure 6. The underlying mechanisms in FPVB modulation by a CBC system. (a1–a4) Far-field intensity distribution of FPVBs with different topological charges of $l = 1.2, 1.4, 1.6$ and 1.8 , respectively. (b1–b4) Far-field intensity distribution of FPVBs formed by different numbers of apertures, $N = 24, 36, 48$ and 60 , respectively. (c) The relationships between the number of apertures and the maximum available gaps. (d1,d2) the results of the far-field intensity distribution formed by 36 apertures. (e1,e2) the results of the far-field intensity distribution modulated by 96 apertures.

3.3. Generation of PVBs by Employing a Tilting Phase in a CBC System

Furthermore, another efficient phase-controlling method for the generation of PVBs in a CBC system is proposed in this section. That is, a tilting phase could be employed due to its similarities to an axial prism phase. Shown in Figure 7(a1–a3) is the near-field phase tilting distribution of PVBs with topological charges of $l = 1, 2$ and 3 at the condition of $r = 150$, where r is utilized to represent the period of the phase change. The corresponding far-field intensity and phase are displayed in Figure 7(b1–b3) and Figure 7(c1–c3), respectively. These results illustrate that PVBs are successfully generated by employing a tilting phase, in good agreement with theory.

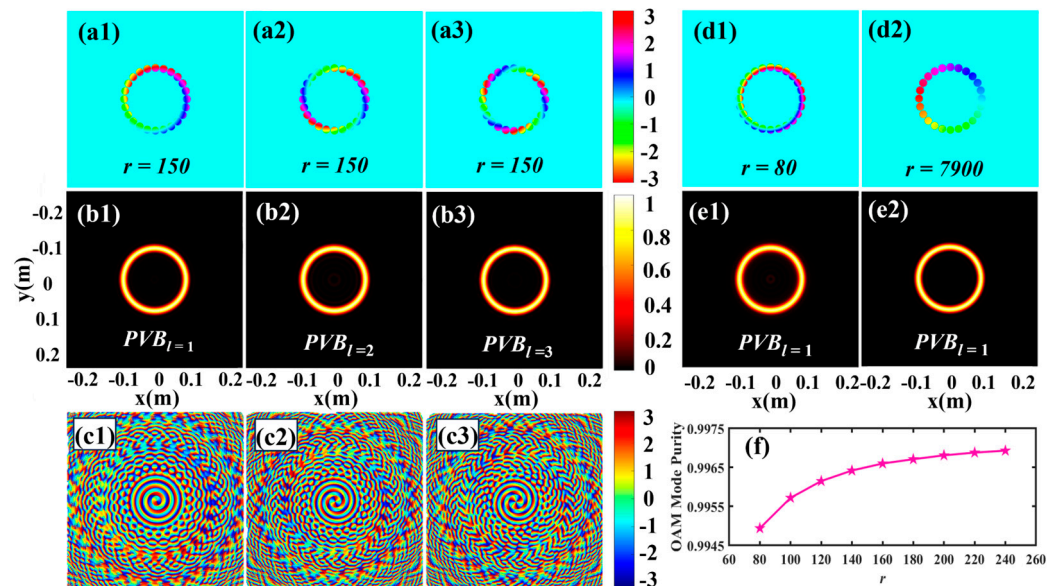


Figure 7. The generation of PVBs by employing a tilting phase in a CBC system. (a1–a3) Near-field phase distribution; (b1–b3) far-field intensity and (c1–c3) phase distribution of PVBs with topological charges of $l = 1, 2$ and 3 at $r = 150$. (d1,d2) Near-field phase and (e1,e2) far-field intensity distribution of PVBs differing from periods r . (f) The relationship between the OAM mode purity and periods r .

To figure out how varied periods of the phase influence the performance of PVBs, a value of r ranging from 80 to 7900 was set and the corresponding OAM mode purity was calculated. The OAM mode purity is at its lowest point when r is 80 (99.49%) in Figure 7(d1), and it reaches its highest point (99.73%) when r is 7900 in Figure 7(d1). Simultaneously, the diameter suffers a slight change from 0.1777 to 0.1772 m as $l = 1$ in Figure 7(e1,e2).

Although the OAM mode purity will be higher than before when the varied periods of the phase increase, as seen in Figure 7f, the actual variation is still limited to the range of 0.3%. When the value of r is large enough, the phase distribution is closer to the ideal spiral phase, and such a phenomenon matches well with the improved OAM mode purity. Note that these results are obtained at the same filtering threshold of 0.07 m.

3.4. Generation and Modulation of FPVBs via a Tilting Phase

With the fractional titling phase controlled, the number of appearing gaps could be modulated according to the integer part of the fraction value. In Figure 8(a1–a5), the near-field phase distributions with varied integer parts were set to 1, 2, 3, 4 and 5, respectively, and they are consistent with the number of gaps in Figure 8(b1–b5). However, due to the limited apertures (36), a number of gaps larger than five is not allowed. These results revealed that multiple gaps can also be flexibly modulated by the tilting phase and they are achieved at the same filtering threshold of 0.065 m.

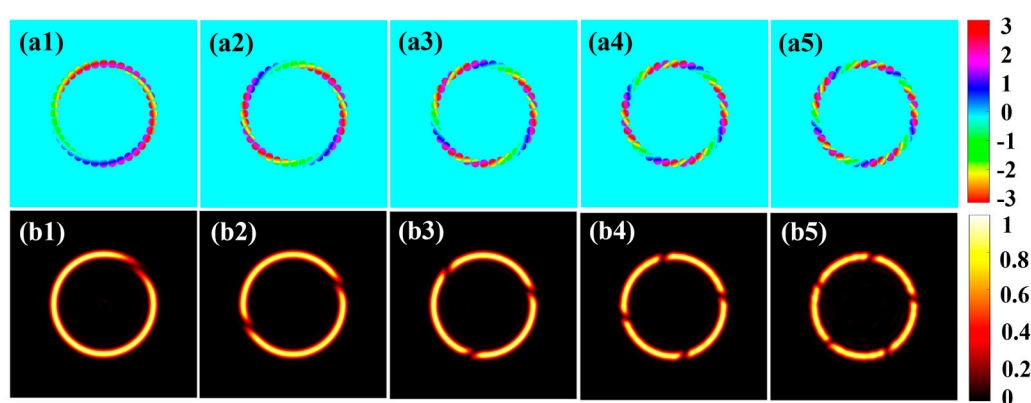


Figure 8. The relationship between the modulated tilting phase and the number of gaps. (a1–a5) Near-field phase distribution and (b1–b5) far-field intensity distribution of FPVBs with different gaps.

With two such different phase control methods, the generation and modulation of PVBs and FPVBs are both flexibly realized. Meanwhile, there are still some differences between these two methods. On the one hand, the advantage of the piston phase control method is that it will be much easier to realize in a practical CBC system, leading to a reduced cost and complexity while retaining a comparable performance of PVBs to that achieved by the tilting phase. On the other hand, the advantage of the tilting phase control method is that the edges of the gaps seem to be smoother than those obtained by employing the piston phase, enabling more gaps to be achieved under the condition of the same number of apertures. Thus, these two methods could be chosen by considering the specific conditions for convenience.

4. Conclusions

To sum up, this work provides efficient strategies to generate PVBs and FPVBs in a CBC system. By employing piston phase and tilting phase control methods, the numerical analysis results demonstrate that both PVBs and FPVBs can be flexibly modulated under these two conditions. The generated PVBs not only exhibit a high OAM mode purity exceeding 99%, but can also be easily transformed into FPVBs with controllable gaps. Moreover, the relationships between filtering thresholds and the parameters of the PVBs have been fully discussed, thereby facilitating the generation of PVBs with enhanced performances. Thus, CBC technology shows promising potential in achieving high-power structured beams and is applicable to laser beam shaping, which will be hopefully applied in diverse fields, for example, particle trapping, optical communication and so on.

Author Contributions: B.S.: conceptualization, investigation, methodology, software, formal analysis, writing—original draft preparation; Y.Z.: visualization, supervision, writing—review and editing; H.C.: visualization; S.T.: numerical analysis; J.X.: project administration; J.L.: project administration; P.Z.: supervision, writing—review and editing. All authors have read and agreed to the published version of the manuscript.

Funding: This research was funded by National Natural Science Foundation of China, grant number 62305388, and the Postgraduate Scientific Research Innovation Project of Hunan Province, grant number QL20230007.

Institutional Review Board Statement: Not applicable.

Informed Consent Statement: Not applicable.

Data Availability Statement: Data are contained within the article.

Conflicts of Interest: The authors declare no conflicts of interest.

References

1. Ostrovsky, A.S.; Rickenstorff-Parrao, C.; Arrizón, V. Generation of the “perfect” optical vortex using a liquid-crystal spatial light modulator. *Opt. Lett.* **2013**, *38*, 534–536. [[CrossRef](#)] [[PubMed](#)]
2. García-García, J.; Rickenstorff-Parrao, C.; Ramos-García, R.; Arrizón, V.; Ostrovsky, A.S. Simple technique for generating the perfect optical vortex. *Opt. Lett.* **2014**, *39*, 5305–5308. [[CrossRef](#)] [[PubMed](#)]
3. Li, X.; Ma, H.; Yin, C.; Tang, J.; Li, H.; Tang, M.; Wang, J.; Tai, Y.; Li, X.; Wang, Y. Controllable mode transformation in perfect optical vortices. *Opt. Express* **2018**, *26*, 651–662. [[CrossRef](#)]
4. Zhu, F.; Huang, S.; Shao, W.; Zhang, J.; Chen, M.; Zhang, W.; Zeng, J. Free-space optical communication link using perfect vortex beams carrying orbital angular momentum (OAM). *Opt. Commun.* **2017**, *396*, 50–57. [[CrossRef](#)]
5. Villalba, N.; Melo, C.; Ayala, S.; Mancilla, C.; Valenzuela, W.; Figueroa, M.; Baradit, E.; Lin, R.; Tang, M.; Walborn, S.P.; et al. Transmission of optical communication signals through ring core fiber using perfect vortex beams. *Opt. Express* **2023**, *31*, 40113–40123. [[CrossRef](#)] [[PubMed](#)]
6. Wang, S.; Xu, J.; Yang, Y.; Cheng, M. Optimization of wireless optical communication using perfect vortex beam. *Opt. Commun.* **2024**, *556*, 130258. [[CrossRef](#)]
7. Wang, G.; Weng, X.; Kang, X.; Li, Z.; Chen, K.; Gao, X.; Zhuang, S. Free-space creation of a perfect vortex beam with fractional topological charge. *Opt. Express* **2023**, *31*, 5757–5766. [[CrossRef](#)] [[PubMed](#)]
8. Chen, M.; Mazilu, M.; Arita, Y.; Wright, E.M.; Dholakia, K. Dynamics of microparticles trapped in a perfect vortex beam. *Opt. Lett.* **2013**, *38*, 4919–4922. [[CrossRef](#)] [[PubMed](#)]
9. Diouf, M.; Harling, M.; Yessenov, M.; Hall, L.A.; Abouraddy, A.F.; Toussaint, K.C. Space-time vector light sheets. *Opt. Express* **2021**, *29*, 37225–37233. [[CrossRef](#)] [[PubMed](#)]
10. Diouf, M.; Lin, Z.; Harling, M.; Toussaint, K.C. Demonstration of speckle resistance using space–time light sheets. *Sci. Rep.* **2022**, *12*, 14064. [[CrossRef](#)]
11. Vaity, P.; Rusch, L. Perfect vortex beam: Fourier transformation of a Bessel beam. *Opt. Lett.* **2015**, *40*, 597–600. [[CrossRef](#)] [[PubMed](#)]
12. Kotlyar, V.V.; Kovalev, A.A.; Porfirev, A.P. Optimal phase element for generating a perfect optical vortex. *J. Opt. Soc. Am. A* **2016**, *33*, 2376–2384. [[CrossRef](#)] [[PubMed](#)]
13. Arrizón, V.; Ruiz, U.; Sánchez-de-la-Llave, D.; Mellado-Villaseñor, G.; Ostrovsky, A.S. Optimum generation of annular vortices using phase diffractive optical elements. *Opt. Lett.* **2015**, *40*, 1173–1176. [[CrossRef](#)] [[PubMed](#)]
14. Tkachenko, G.; Chen, M.; Dholakia, K.; Mazilu, M. Is it possible to create a perfect fractional vortex beam? *Optica* **2017**, *4*, 330–333. [[CrossRef](#)]
15. Li, L.; Chang, C.; Yuan, X.; Yuan, C.; Feng, S.; Nie, S.; Ding, J. Generation of optical vortex array along arbitrary curvilinear arrangement. *Opt. Express* **2018**, *26*, 9798–9812. [[CrossRef](#)] [[PubMed](#)]
16. Long, J.; Chen, X.; Chang, Q.; Hou, T.; Deng, Y.; Zhang, J.; Su, R.; Ma, Y.; Ma, P.; Zhou, P. Controllable customization of optical vortex lattices with coherent laser array. *Opt. Laser Technol.* **2023**, *160*, 109045. [[CrossRef](#)]
17. Kurti, R.; Halterman, K.; Shori, R.; Wardlaw, M. Discrete cylindrical vector beam generation from an array of optical fibers. *Opt. Express* **2009**, *17*, 13982–13988. [[CrossRef](#)] [[PubMed](#)]
18. Adamov, E.V.; Aksenov, V.P.; Atuchin, V.V.; Dudorov, V.V.; Kolosov, V.V.; Levitsky, M.E. Laser beam shaping based on amplitude-phase control of a fiber laser array. *OSA Contin.* **2021**, *4*, 182–192. [[CrossRef](#)]
19. Long, J.; Jin, K.; Chen, Q.; Chang, H.; Chang, Q.; Ma, Y.; Wu, J.; Su, R.; Ma, P.; Zhou, P. Generating the 1.5 kW mode-tunable fractional vortex beam by a coherent beam combining system. *Opt. Lett.* **2023**, *48*, 5021–5024. [[CrossRef](#)] [[PubMed](#)]
20. Veinhard, M.; Bellanger, S.; Daniault, L.; Fsaifes, I.; Bourderionnet, J.; Larat, C.; Lallier, E.; Brignon, A.; Chanteloup, J.-C. Orbital angular momentum beams generation from 61 channels coherent beam combining femtosecond digital laser. *Opt. Lett.* **2021**, *46*, 25–28. [[CrossRef](#)] [[PubMed](#)]

21. Adamov, E.V.; Aksenov, V.P.; Dudorov, V.V.; Kolosov, V.V.; Levitskii, M.E. Controlling the spatial structure of vector beams synthesized by a fiber laser array. *Opt. Laser Technol.* **2022**, *154*, 108351. [[CrossRef](#)]
22. Lin, D.; Carpenter, J.; Feng, Y.; Jain, S.; Jung, Y.; Feng, Y.; Zervas, M.N.; Richardson, D.J. Reconfigurable structured light generation in a multicore fibre amplifier. *Nat. Commun.* **2020**, *11*, 3986. [[CrossRef](#)] [[PubMed](#)]
23. Chu, X.; Liu, Z.; Zhou, P. Generation of a high-power Airy beam by coherent combining technology. *Laser Phys. Lett.* **2013**, *10*, 125102. [[CrossRef](#)]
24. Chu, X. Analytical study on the self-healing property of Bessel beam. *Eur. Phys. J. D* **2012**, *66*, 259. [[CrossRef](#)]
25. Yu, T.; Xia, H.; Xie, W.; Xiao, G.; Li, H. The generation and verification of Bessel-Gaussian beam based on coherent beam combining. *Results Phys.* **2020**, *16*, 102872. [[CrossRef](#)]
26. Chu, X.; Sun, Q.; Wang, J.; Lü, P.; Xie, W.; Xu, X. Generating a Bessel-Gaussian beam for the application in optical engineering. *Sci. Rep.* **2015**, *5*, 18665. [[CrossRef](#)] [[PubMed](#)]
27. Ju, P.; Fan, W.; Gao, W.; Li, Z.; Gao, Q.; Jiang, X.; Zhang, T. Phase control scheme of the coherent beam combining system for generating perfect vectorial vortex beams assisted by a Dammann vortex grating. *Opt. Express* **2023**, *31*, 22372–22384. [[CrossRef](#)] [[PubMed](#)]
28. Ju, P.; Fan, W.; Gao, W.; Li, Z.; Gao, Q.; Li, G.; Jiang, X.; Zhang, T. Generation of perfect vectorial vortex beams by employing coherent beam combining. *Opt. Express* **2023**, *31*, 11885–11898. [[CrossRef](#)]
29. Woerdemann, M.; Alpmann, C.; Esseling, M.; Denz, C. Advanced optical trapping by complex beam shaping. *Laser Photonics Rev.* **2013**, *7*, 839–854. [[CrossRef](#)]
30. Kovalev, A.A.; Kotlyar, V.V.; Porfirev, A.P. A highly efficient element for generating elliptic perfect optical vortices. *Appl. Phys. Lett.* **2017**, *110*, 261102. [[CrossRef](#)]

Disclaimer/Publisher’s Note: The statements, opinions and data contained in all publications are solely those of the individual author(s) and contributor(s) and not of MDPI and/or the editor(s). MDPI and/or the editor(s) disclaim responsibility for any injury to people or property resulting from any ideas, methods, instructions or products referred to in the content.